



# Critical Angle and Fundamental Frequency of Symmetric Airfoils at Low Reynolds Numbers

D. F. Kurtulus<sup>†</sup>

*METU Aerospace Engineering Department, 06800, Ankara, Turkey*

<sup>†</sup>Corresponding Author Email: [kurtulus@metu.edu.tr](mailto:kurtulus@metu.edu.tr)

(Received June 13, 2021; accepted November 14, 2021)

## ABSTRACT

The unsteady vortex evolution of NACA 0012 airfoil is numerically investigated at low angles of attack ranging from 0° to 10° where the separation is performed from the trailing edge. The Reynolds number ranges between 1000 and 4000. The laminar separation bubble at the trailing edge is observed and the main flow features are presented. It is found that, the increase of the angle of attack and Reynolds number result higher lift to drag ratio by an extensive decrease of the drag coefficient below 8° angle of attack. The transition from the steady condition to periodic force evolution has been revealed with a detailed flow field analysis at different angles of attack and Reynolds numbers. The critical angle is defined as the angle of attack where the onset of oscillations starts with a dominant fundamental frequency of oscillation. The angle of attack where the laminar separation bubble (LSB) is observed is also revealed in the current study. Both the LSB formation angle and the critical angle of attack is found to decrease with the increase of the Reynolds number from 1000 to 4000.

**Keywords:** Micro air vehicles; Vortex shedding; Unsteady aerodynamics.

## NOMENCLATURE

$c$	chord	$p_0$	free-stream static pressure
$C_f$	skin friction coefficient	$q$	dynamic pressure ( $1/2\rho U_0^2$ )
$C_p$	pressure coefficient	$Re$	Reynolds number
$C_l$	instantaneous lift coefficient	$St$	Strouhal number ( $fc/U_0$ )
$\overline{C_l}$	mean lift coefficient	$U_0$	freestream velocity
$C_d$	instantaneous drag coefficient	$\vec{V}$	total velocity vector
$\overline{C_d}$	mean drag coefficient	$\alpha$	angle of attack
$D'$	drag per unit span	$\alpha_{cr}$	critical angle of attack
$dt$	time step	$\alpha_{LSB}$	LSB formation angle of attack
$f_{cr}$	fundamental frequency at $\alpha_{cr}$	$\Delta t$	time increment
$L'$	lift per unit span	$\rho$	fluid density
$p$	static pressure	$\nu$	kinematic viscosity

## 1. INTRODUCTION

The advance of technologies increases the interest to micro and even nano air vehicles which are imitating the flights of birds and insects. Reynolds number regimes for birds are in the range of  $10^4$  to  $10^5$  for birds and lower than  $10^4$  for insects (Traub and Coffman 2019). Reynolds numbers of different insects which have also hovering capability are order of  $10-10^4$ . For example, fruit fly has a Reynolds number as low as  $\sim 150$  in hover, similarly honeybee has  $Re \sim 1200$ , dragonfly has  $Re \sim 2000$ , hawkmoth has  $Re \sim 6000$  (Han *et al.* 2014).

The low Reynolds number flows also take the interest due to the unsteady aerodynamics around the wind turbine blades. DNS simulations with spectral/hp element method are used by Nakhchi *et al.* (2021) to investigate the transition to turbulence and the laminar separation bubble around NACA4412 airfoil as a wind turbine blade airfoil in the Reynolds number range of  $2.5 \times 10^4 - 1.5 \times 10^5$  and the angle of attack range of  $0^\circ-16^\circ$ .

The airfoil performance is highly affected by the unsteadiness of the flow behind the airfoil (Lee and Huang 1998). At low angles of attack, the separation is observed to start from the trailing edge

of the airfoil at low Reynolds numbers which is also denoted by Huang *et al.* (2001). A laminar separation bubble (LSB) is observed at the suction surface of the airfoil (Jones 1933). The reattachment point of the LSB is found to be unsteady which is also denoted to be one of the reasons of the shedding of the vortical structures from LSB (Wattmuff 1999; Traub and Cooper 2008; Eljack *et al.* 2020, 2021). The investigation of the vortical patterns also reveals the high amplitudes oscillations in aerodynamic forces at these low Reynolds numbers.

Ohtake *et al.* (2007) measured the aerodynamic forces and pitching moment with respect to quarter chord point of NACA 0012 airfoil in a 0.3 m x 0.3 m cross section wind tunnel at Reynolds numbers in the range of  $1 \times 10^4$  to  $1 \times 10^5$ . Council *et al.* (2013) have done a comparative study of two airfoils (NACA 0012 and SD 7003) at low Reynolds numbers ranging from  $4.8 \times 10^4$  to  $2.5 \times 10^5$  and at angles of attack ranging from  $0^\circ$  to  $8^\circ$  using unsteady RANS shear-stress transport  $\gamma$ - $Re_\theta$  model with different turbulence intensities and the ANSYS CFX solver. They found that by the angle of attack and Reynolds number increase, the laminar-separation bubbles shrank and moves toward the leading edge. Council *et al.* (2013) also compared their results and found similar results with the experimental data of Ohtake *et al.* (2007). Cleaver *et al.* (2012) perform experiments on a NACA 0012 airfoil of dimensions 0.1 m chord and 0.3 m span in a free-surface closed-loop water tunnel with a turbulence intensity less than 0.5%. The lift force measurements for the stationary 2D NACA 0012 airfoil are presented for  $Re = 10,000, 20,000,$  and  $30,000$ . They denoted that the lift curves for  $Re \geq 20,000$  are typical of leading-edge stall, and those for  $Re < 20,000$  are typical of laminar trailing-edge stall (Cleaver *et al.* 2012). For  $Re < 20,000$ , as a result of the trailing-edge stall, the peak of the lift coefficient is more rounded and diminishes slightly. This phenomena is also observed by Huang and Lin (1995) who have experimentally investigated the flow patterns and characteristics of vortex shedding and shear-layer instability of a NACA 0012 cantilever wing using smoke wire and surface oil flow techniques. They have also measured the frequencies of the shed vortices in the wake region and the instability waves developed on the separated shear layers by using two one-component hot-wire anemometers (Huang and Lin 1995).

Kurtulus (2015, 2016) using laminar unsteady RANS simulations showed wake patters at  $Re=1000$  for steady uniform flows around NACA 0012 and NACA 0002 airfoils at different incidence angles and classified them into five different modes (Rossi *et al.* 2018, Durante *et al.* 2020). These results are also compared with small amplitude pitching NACA 0012 airfoil (Kurtulus 2018; Kurtulus 2019). Rossi *et al.* (2018) and Durante *et al.* (2020) show that the classification of the wake structures behind NACA 0010 airfoil are similarly visualized for Reynolds number ranging from 100 to 3000 and at different incidence angles.

In the present study, the focus is given to low angles of attack to understand the trailing edge separation phenomena at low Reynolds numbers of 1000 to 4000. The novelty of the current paper is to show the effect of the Reynolds number at these low values where the data is not available in the literature to the best knowledge of the author on the instantaneous and mean flow fields and the aerodynamic coefficients for angles of attack up to  $10^\circ$ .

## 2. METHODOLOGY

Unsteady, incompressible, laminar and two dimensional Navier-Stokes equations are used for the numerical simulations as is given by Eq. (1) and Eq. (2). A commercial software (ANSYS Fluent v14.0) which is a finite volume solver is used to obtain current results. SIMPLE-type fully implicit algorithm is used with pressure-velocity coupling and all the time and spatial solutions are selected to be second order accurate.

$$\bar{\nabla} \cdot \bar{V} = 0 \quad (1)$$

$$\frac{\partial \bar{V}}{\partial t} + (\bar{V} \cdot \bar{\nabla}) \bar{V} = -\frac{1}{\rho} \bar{\nabla} p + \nu \nabla^2 \bar{V} \quad (2)$$

The symmetric airfoils are pivoted from the quarter chord location and they are rotated with the corresponding angle of attack before the grid domain is formed. The field is composed of two domains, one close to the airfoil and the second one outside of the inner domain which extends 19c away of the airfoil towards both upstream and downstream (Fig. 1).

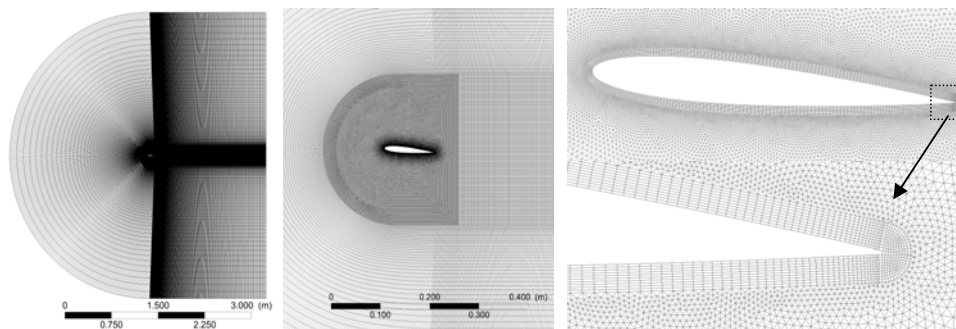


Fig. 1. Medium mesh used in the present study (NACA 0012,  $\alpha=5^\circ$ ).

Mesh	Re	Laminar/turbulent analysis	Nodes around airfoil	Number of elements	$\Delta t$ [s]	First cell spacing of BL	$\bar{C}_l$	$\bar{C}_d$
Coarse	1000	Laminar	150	93915	0.005	0.002c	0.4158	0.1648
Medium	1000	Laminar	300	194961	0.005	0.002c	0.4180	0.1650
Fine	1000	Laminar	500	248168	0.005	0.0015c	0.4188	0.1651
Medium	1000	Laminar	300	194961	0.01	0.002c	0.4182	0.1651
Medium	1000	Laminar	300	194961	0.0005	0.002c	0.4179	0.1650
Mittal and Tezduyar (1994)	1000	Laminar	N/A	23600	0.01	0.002c	0.4192	0.1647
Medium	2000	Laminar	300	194961	0.005	0.002c	0.4712	0.1528
Medium	4000	Laminar	300	194961	0.005	0.002c	0.9686	0.1994
Medium	4000	k- $\omega$ SST	300	194961	0.005	0.002c	0.9686	0.1994
Fine	4000	Laminar	500	248168	0.005	0.0015c	0.9823	0.1987
Fine	4000	k- $\omega$ SST	500	248168	0.005	0.0015c	0.9826	0.1987

**Table 1** Grid and time refinement studies for NACA 0012 airfoil at  $\alpha=10^\circ$ .

With the preprocessor program, the airfoil is rotated for the given angle of attack in the inner region by keeping the outer domain and wake region fixed with the same structured grid. Three different meshes are compared for  $10^\circ$ ,  $20^\circ$ ,  $35^\circ$  and  $40^\circ$  angles of attack in previous studies of the author and the results with medium and fine meshes are found to be very close to each other and also to the numerical simulations available in the literature (Kunz and Kroo 2000; Hoarau *et al.* 2003; Mittal and Tezduyar 1994; Liu *et al.* 2012; Khalid and Akhtar 2012; Suzuki *et al.* 2009). The boundary layer has a first spacing of 0.002c for the medium mesh configuration selected whose number of elements are in the order of  $2 \times 10^5$ . The number of nodes around the airfoil is 300 for the medium mesh configuration (Fig. 1).

A time refinement study has also been performed (Kurtulus 2015, 2016) and a time increment of  $\Delta t=0.005s$  is selected for the simulations. The average quantities are obtained in the interval of  $50s \leq t \leq 100s$  where quasi-steady solutions are obtained. Mittal and Tezduyar (1994) used for Reynolds numbers 1000 and 5000, a mesh with 23600 elements and 23900 nodes around NACA 0012 airfoil. Their unsteady numerical simulation method is based on the Deforming-Spatial-Domain/Stabilized-Space-Time finite element formulation. The mean values of Mittal and Tezduyar (1994) in comparison with the current study grid refinement results are also tabulated in Table 1. Their results are found to be very similar with the results obtained in the current study. In the current study, fine mesh is also used for the highest Reynolds number and highest angle of attack investigated (Re=4000 and  $\alpha=10^\circ$ ). The mean aerodynamic force coefficients are found to be very close to the medium mesh results as shown also in Table 1.

The comparison of the mean aerodynamic force coefficients with the data available in literature (Mittal and Tezduyar 1994; Liu *et al.* 2012; Khalid and Akhtar 2012; Sunada *et al.* 1997) are given in Fig. 2. Mean lift coefficient for NACA 0012 at Re=1000 give very similar results with data available in literature (Liu *et al.* 2012; Khalid and Akhtar 2012). The results at Re=4000 are also

compared with the experimental data of Sunada *et al.* (1997) which are also available in Cleaver *et al.* (2012). Sunada *et al.* (1997), using a load cell, examined experimentally in a water tank the aerodynamic forces of fifteen different airfoil shapes one of them being NACA 0012 airfoil at Re=4000. Sunada *et al.* (1997) also observed that the roughness of the airfoils tested during the experiments does not affect the aerodynamic performance of the airfoils and this could be explained by the fact that this Reynolds number is far below the transition Reynolds number as is emphasized by Schmitz (1967).

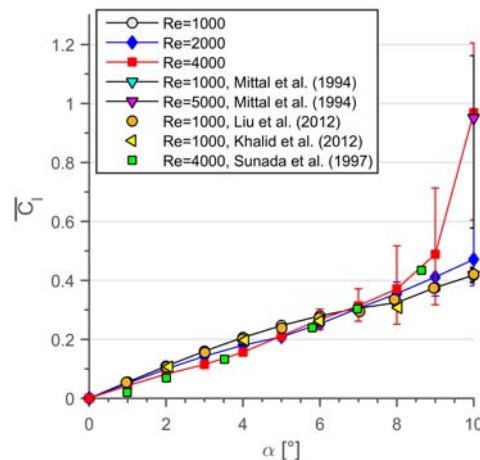


**Fig. 2.** Mean lift coefficients in comparison with the literature data.

The transition is defined as the passage from laminar and separated (subcritical) flow on the upper surface boundary layer of the airfoil to the turbulent and attached flow (supercritical). Schmitz (1967) has performed wind tunnel test with force measurements on the Reynolds number ranges of 21000 to 168000 using 5 different airfoils. He denoted that for  $Re < 150000$ , the airfoil has a critical range where the boundary layer become turbulent and the previously separated laminar boundary layer attaches. This situation results a sudden increase in lift coefficient and a decrease in the drag coefficient and a high  $C_l/C_d$  ratio compared to

Reynolds number regimes lower than transition Reynolds number.

The transition Reynolds number for NACA N60 airfoil at  $\alpha=6^\circ$  was found to be at  $Re=63000$  where  $C_l/C_d$  ratio in the supercritical condition becomes three times that of the subcritical case. From the stagnation point over the upper surface the airfoil, a negative pressure region is formed which is the main lift contribution region. From the minimum pressure region until the trailing edge, the pressure increases on the upper surface. The deceleration of the flow and the pressure increase can cause separation of the flow on the upper surface. On the lower surface of the airfoil, from the stagnation point to the trailing edge, and on the upper surface of the airfoil from the stagnation point to the pressure minimum, there is a tendency to maintain the laminar boundary flow due to the pressure increase and accelerated flow (Schmitz 1967). For higher Reynolds numbers, above transition Reynolds number, from the minimum pressure location until the trailing edge, because of the pressure increase, there is also a tendency to transition to turbulence (Schmitz 1967).

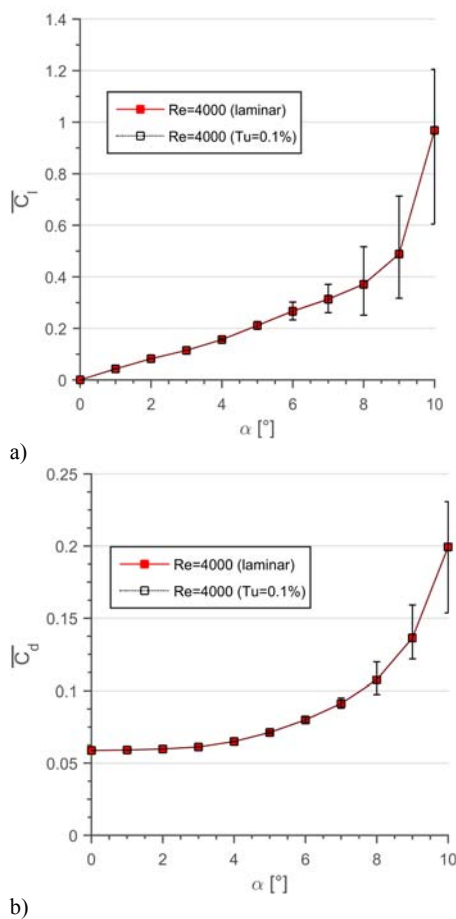


**Fig. 3. Mean lift coefficient (a) and mean drag coefficient (b) at  $Re=4000$  comparing laminar and  $k-\omega$  SST turbulence model ( $Tu=0.1\%$ ) solutions.**

A previous numerical study for lower thickness to chord ratios have been performed by Kunz and Kroo (2000) with laminar, two-dimensional incompressible Navier-Stokes solver for Reynolds numbers from 1000 to 12000. All their numerical calculations use a C-grid topology with either 256 by 64 cells or 512 by 128 cells. They also denoted that if there is no separation in the flow and the flowfield will be entirely laminar at these Reynolds numbers. Even from slight to moderate separation for  $Re<10000$  will result a laminar reattachment (Kunz and Kroo 2000).

The laminar results of  $Re=4000$  are also compared with  $k-\omega$  SST turbulence model with low Reynolds number correction using a low turbulence intensity of 0.1% for angles of attack of  $0^\circ$  to  $10^\circ$  and the aerodynamic force coefficients are found to be very close to the laminar simulations for this Reynolds number (Fig. 3). The laminar and turbulent analysis are also compared using fine mesh for the maximum angle of attack studied in the current study ( $\alpha=10^\circ$ ) as tabulated in Table 1. and results are also found to be close to each other.

The mean pressure coefficient and the mean skin friction coefficient along the x direction are also shown in Fig. 4 for  $Re=4000$  and maximum angle of attack studied in the current study ( $\alpha=10^\circ$ ). The medium mesh and fine mesh solutions are observed to be very close to each other. The distributions are also compared for laminar and turbulent solutions. The difference between the mean  $C_p$  and mean  $C_f$  coefficients all along the airfoil are also presented in Fig. 4c and Fig. 4d, respectively. The main differences are observed to be at the leading edge and then at the trailing edge of the airfoil.

### 3. RESULTS

The aerodynamic forces are highly unsteady depending on the separation type observed at the suction side of the airfoil. A detailed analysis is needed to understand the vortex shedding phenomena and oscillations of the aerodynamic forces at low Reynolds numbers. The amplitude of oscillation for the aerodynamic coefficients are found to increase rapidly with the angle of attack in these Reynolds number intervals.

The minimum and maximum values of the unsteady lift and drag coefficients are presented in Fig. 5 with error bars in addition to the mean values. The oscillations become clear for  $Re=4000$  at critical angle of attack of  $\alpha_{cr}=4^\circ$  and for  $Re=2000$  at  $\alpha_{cr}=6^\circ$ . The wake shedding is found to be  $\alpha_{cr}=8^\circ$  for  $Re=1000$  for NACA 0012 airfoil. The vortex shedding phenomena is highly dependent to angle of attack, Re number and airfoil thickness (Kunz and Kroo 2000, Kurtulus, 2015, 2016; Rossi et al. 2018; Durante et al. 2020). The present study shows the effect of angle of attack and Re number on the onset of these oscillatory conditions. It is found that the lift curve slope at  $\alpha=0^\circ$  decreases with Reynolds number increase from 1000 to 4000 (Fig. 5a). The lift coefficient decreases as the Reynolds number increases from 1000 to 4000 for  $\alpha \leq 4^\circ$ . The lift

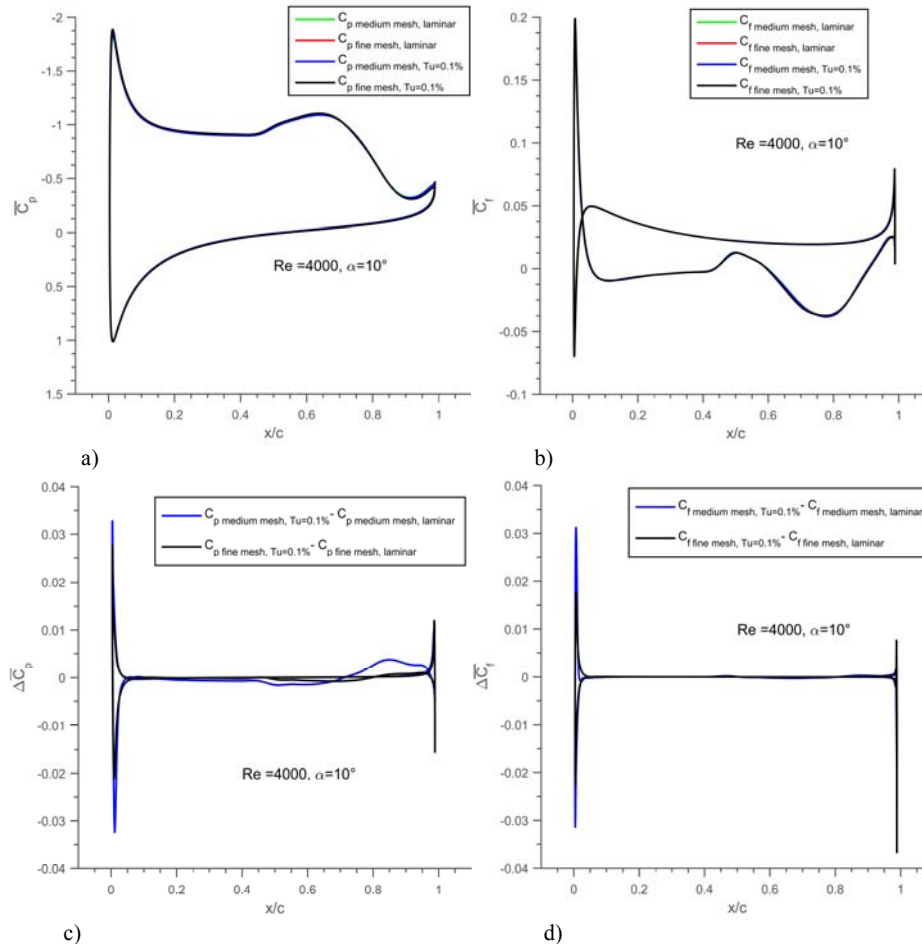


**Fig. 4. Mean pressure coefficient (a), mean skin friction coefficient (b) and the discrepancies between two models  $\Delta C_p$ (c),  $\Delta C_f$  (d) at  $Re=4000$  and  $\alpha=10^\circ$  comparing medium mesh, fine mesh results with laminar solution and  $k-\omega$  SST turbulence model ( $Tu=0.1\%$ ) solution.**

coefficient is found to be almost same for  $\alpha=7^\circ$  for these Reynolds numbers. For  $\alpha>7^\circ$ , the lift coefficients are found to increase with the increase of the Reynolds number.

For the drag coefficient, there is a decrease of the mean values as the Reynolds number increases from 1000 to 4000 as is shown in Fig. 5b until  $9^\circ$  angle of attack. At  $\alpha=9^\circ$  angle of attack,  $Re=4000$  results higher drag coefficient with respect to  $Re=2000$ . At  $\alpha=10^\circ$  angle of attack, the increase of the drag coefficient is sharper and results higher values for  $Re=4000$  compared to both  $Re=2000$  and  $Re=1000$  cases. As a result, a sudden jump of the lift to drag ratio is observed at  $\alpha=10^\circ$ . It should be noted that the turbulent solutions above  $10^\circ$  is found to change the aerodynamic force coefficients so this sudden increase in lift and drag coefficients are found to be as a precursor for the turbulent effects in 2D flows. It is also noted that at this angle of attack the amplitude of oscillations for both lift and drag coefficients are relatively big compared to smaller angles of attack. This phenomena need further investigations therefore the current study is limited

for the results where the laminar solutions are very similar with the turbulent results (see Fig. 3 and Table 1). For all Reynolds number cases investigated, the lift to drag ratio of  $Re=4000$  is found to be the biggest in the angle of attack interval of  $\alpha \in [0^\circ 10^\circ]$ . Fig. 5c shows the Strouhal number based on the frequency ( $f$ ) corresponding to the maximum amplitude of the amplitude spectrum of the unsteady lift coefficient obtained from the Fast Fourier Transformation as a function of the angle of attack and Reynolds number. The results are presented for both below the critical angle of attack (hollow symbols and dashed lines in Fig. 5c) and above the critical angle of attack (filled symbols and solid lines in Fig. 5c). The critical angle of attack is defined as the angle where the onset of oscillation is observed and a very major fundamental frequency can be detected from the amplitude spectrum of the aerodynamic force coefficients who shows oscillatory behaviors. A more detailed discussion for the critical angle of attack is given in the following section. Below the critical angle of attack, there is very low scale frequency amplitudes which does not show a

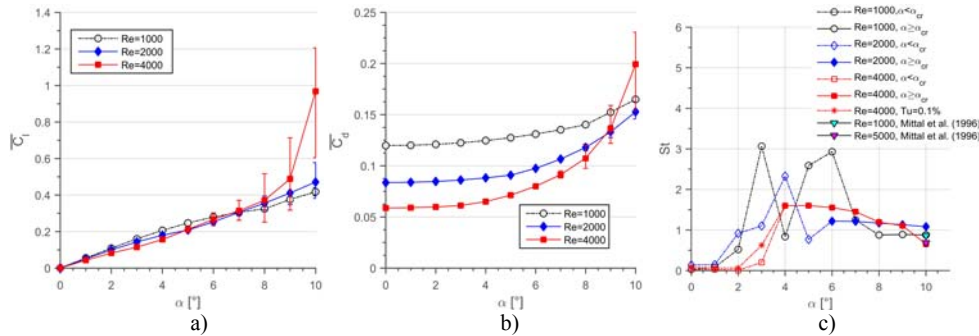


**Fig. 5** The mean lift coefficient (a), the mean drag coefficient (b) and Strouhal number (c) for NACA 0012 airfoil at low Reynolds numbers.

dominant frequency. Some of these low scale frequencies below the critical angle of attack could be due to the internal corrections of the commercial solver aimed at reaching the convergence of the computations.

In the current study, the maximum frequency amplitude is also selected for the angles of attack below the critical angle to obtain Strouhal number where the wakes are not even shed and the aerodynamic force coefficients are not in a clear oscillatory behavior (see Fig. 15a for amplitude spectrum of lift coefficient at  $\alpha=3^\circ$ ). For these low angles of attack a persistent laminar separation bubble (LSB) is observed.

The mean lift and drag coefficient variations with respect to Reynolds number are also presented in Fig. 6. It is clearer from Fig. 6 that as Reynolds number increases, the lift coefficient decreases for  $\alpha \leq 4^\circ$ . For  $5^\circ \leq \alpha \leq 6^\circ$ , the minimum mean lift coefficient is obtained at  $Re=2000$ , so the mean lift coefficient decrease and then increase in the  $Re$  number range of 1000 to 4000. The mean lift coefficient is found to be almost constant for  $\alpha=7^\circ$  for Reynolds numbers investigated. For  $\alpha \geq 8^\circ$ , the mean lift coefficient is found to increase with the increase of  $Re$  number. A very sharp increase in mean lift coefficient is observed for  $\alpha=10^\circ$ . The mean drag coefficient is found to decrease with the increase of the Reynolds number for the angles of attack less than equal to  $8^\circ$ . For  $\alpha=9^\circ$  and  $\alpha=10^\circ$ , the minimum mean drag coefficient is obtained at  $Re=2000$ . As the Reynolds number increases both the lift and drag coefficient amplitudes are observed to grow above the critical angles of attack where oscillations exist.

### 3.1 LSB Formation Angle and Critical Angle for the Onset of Oscillations

Oscillation in the aerodynamic coefficients are mainly dependent to the pressure and skin friction distributions on the airfoil which also changes instantaneously by the formation of the laminar separation bubble (LSB). At very low angles of attack, LSB is found to be close to the trailing edge and an increase in the angle of attack causes the separation point to move forward towards the

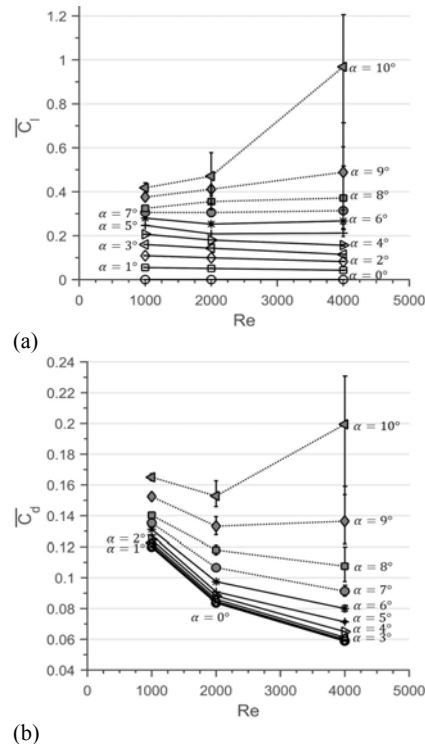


**Fig. 6.** Mean  $C_l$  (a) and mean  $C_d$  (b) of NACA 0012 airfoil at different incidence angles for  $Re=1000, 2000$  and  $4000$ .

leading edge (Fig. 7-Fig. 9). As also denoted by Tani (1964) a further increase of the angle of attack moves the separation point so far forward that the flow no longer reattaches to the surface within a short distance therefore the bubble has broken down or burst. Fig. 7 to Fig. 9 show the instantaneous pressure coefficient contours and streamlines at different angles of attack from  $Re=1000$  to  $Re=4000$  at  $t=100s$ . Below the critical angle of attack, it was also shown that the instantaneous and mean velocity fields reveals same vortex patterns (Kurtulus 2015) as is also shown in Fig. 7.

It is clear from Fig. 7-Fig. 9 that, for  $\alpha=3^\circ$ , LSB at the trailing edge is generated and grow as the  $Re$

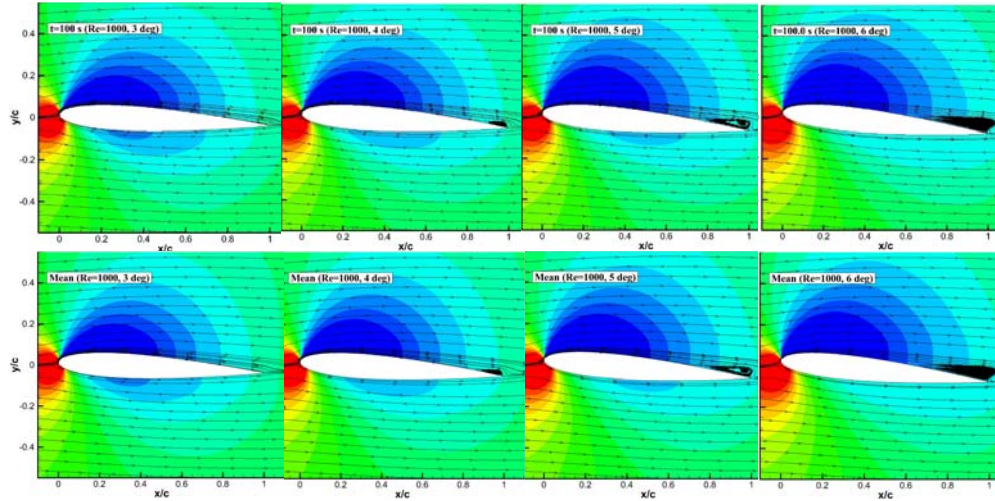


**Fig. 7.** Instantaneous ( $t=100s$ , 1<sup>st</sup> row) and mean (2<sup>nd</sup> row) pressure coefficient contours and streamlines for  $Re=1000$  at  $3^\circ \leq \alpha \leq 6^\circ$ .

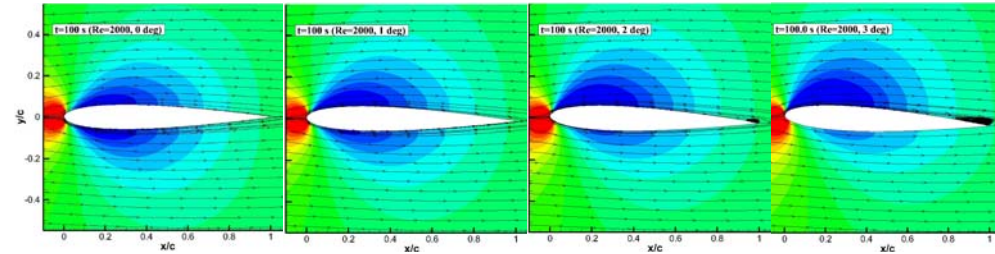


**Fig. 8.** Instantaneous ( $t=100s$ ) pressure coefficient contours and streamlines for  $Re=2000$  at  $0^\circ \leq \alpha \leq 3^\circ$ .

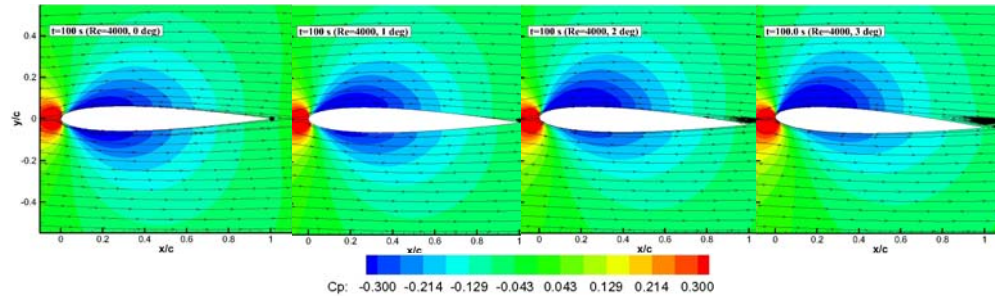


**Fig. 9.** Instantaneous ( $t=100s$ ) pressure coefficient contours and streamlines for  $Re=4000$  at  $0^\circ \leq \alpha \leq 3^\circ$ .

number increases from 1000 to 4000. In addition, its separation point moves towards the leading edge as the Reynolds number increases. Both the mean lift coefficient and the mean drag coefficient are found to decrease with the increase of the Reynolds number from 1000 to 4000 at  $\alpha=3^\circ$  as is also shown in Fig. 6. Although the loss of the mean lift coefficient is not very effective, the drag coefficient is found to sharply decrease even in the presence of a growing LSB at the trailing edge. Figure 10 shows the instantaneous and mean pressure and skin friction coefficient distributions around the NACA 0012 airfoil at  $\alpha=2^\circ$  for the Reynolds number range of 1000 to 4000. The instantaneous and mean distributions are found to be very close to each

other. Skin friction coefficient all along the airfoil surface is found to decrease by the increase of the Reynolds number from 1000 to 4000 (Fig. 10b). No laminar separation bubble is observed at  $Re=1000$  for  $\alpha=2^\circ$ . However when the Reynolds number increases to 2000, LSB is formed at the trailing edge of the airfoil. Trailing edge pressure distribution is found to decrease in magnitude as the Reynolds number increases (Fig. 10a). However, the suction pressure at the leading edge is increased in magnitude as the Reynolds number increases. The lift coefficient slightly decreases with the Reynolds number increase due to the decrease of the discrepancy between the upper and lower surface pressure distributions however, the skin

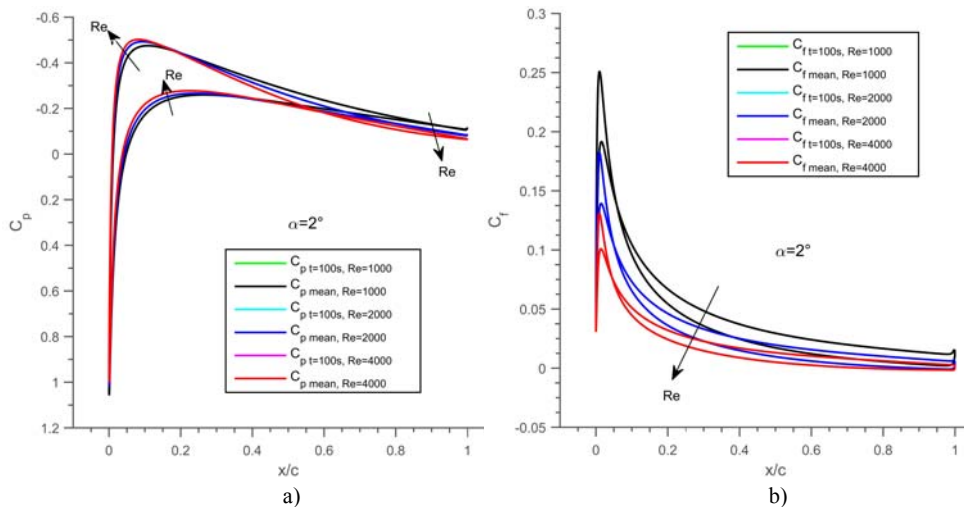


**Fig. 10. Instantaneous ( $t=100s$ ) and mean a)  $C_p$  and b)  $C_f$  distributions around NACA 0012 airfoil at  $\alpha=2^\circ$  for different Reynolds numbers.**

friction coefficient reveals an effective drop of the drag coefficient with the Reynolds number increase.

It is also very well-known that at these low Reynolds numbers separation starts from the trailing edge and as the angle of attack increases the separation point moves towards the leading edge creating a bigger separation bubble (Kunz and Kroo 2000; Kurtulus 2015, Eljack *et al.* 2021).

LSB is first distinguished at an incidence of  $4^\circ$  for  $Re=1000$  and found to persists up to higher angles of attack (Fig. 7). This angle is referred as LSB formation angle in the current study ( $\alpha_{LSB}$ ). At higher angles of attack, for each Reynolds number and airfoil thicknesses, the LSB separation point moves forward towards the leading edge then turns to a leading edge separation which covers the whole airfoil upper surface by the formation also of the secondary, tertiary vortices. This onset of oscillatory behavior in unsteady force coefficients and alternating vortex shedding is referred as critical angle ( $\alpha_{cr}$ ) in the current study and the shedding frequency at this angle of attack is denoted to be the fundamental frequency,  $f_{cr}$ , at the critical angle of attack. The LSB is observed above an *LSB formation angle* and it is found to be stable and persistent characteristic for angles of attack lower than the *critical angle*. Just above the *critical angle*, the vortices are observed to shed alternately and the aerodynamic forces above this angle of attack have almost sinusoidal patterns for the alternating vortex shedding mode conditions (see Fig. 12b and Fig. 14).

In a previous study of Kurtulus (2016), the vortex shedding patterns were classified into five different vortex shedding modes according to the vortex pattern, amplitude spectrum of  $C_l$ , and the longitudinal and lateral spacing of the vortices behind NACA 0002 and NACA 0012 airfoils at  $Re=1000$  considering different angles of attack. Mode 1 which was denoted as “*continuous vortex sheet mode*” is obtained at  $\alpha \leq 8^\circ$  for NACA 0002 and  $\alpha \leq 7^\circ$  for NACA 0012. Mode 2 nominated as

“*alternating vortex shedding mode*” was observed at  $9^\circ \leq \alpha \leq 11^\circ$ ,  $14^\circ \leq \alpha \leq 20^\circ$  for NACA 0002 and  $8^\circ \leq \alpha \leq 22^\circ$  NACA 0012. It is thus noted that the critical angle also represents the angle when this vortex shedding mode changes from Mode 1 to Mode 2. Huang *et al.* (2001) observed an attached flow regime in their experimental study where they noticed an attached flow at the suction surface of NACA 0012 airfoil without a separation or vortical structure at  $\alpha=2^\circ$  and  $Re=1200$ .

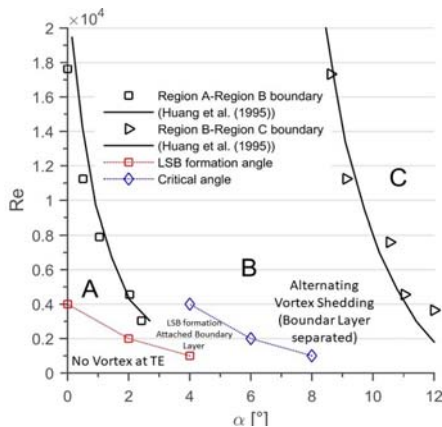
Table 2 shows in summary the LSB formation angle, critical angle and fundamental frequency for Reynolds numbers between 1000 and 4000 for the case investigated in the current study. No vortex is detected on the NACA 0012 airfoil surface for  $\alpha \leq 3^\circ$  for  $Re=1000$  so the *LSB formation angle* is found to be  $4^\circ$  at  $Re=1000$  for NACA 0012 airfoil (Fig. 7). However, LSB formation is detected at  $\alpha=0^\circ$  at  $Re=4000$  for the same airfoil (Fig. 9). Since  $\alpha=0^\circ$ , is a symmetric condition both for the upper surface and the lower surface of the airfoil, the same trailing edge vortex is observed. Fundamental frequency is found to increase with the Reynolds number from 1.28 Hz for  $Re=1000$  to 9.34 Hz for  $Re=4000$ . Both the LSB formation angle and critical angle decreases with the increase of the Reynolds number.

**Table 2 LSB formation angles and critical angles for NACA 0012 airfoil at low Reynolds numbers**

NACA 0012	Re=1000	Re=2000	Re=4000
<i>LSB formation angle</i> ( $\alpha_{LSB}$ )	$4^\circ$	$2^\circ$	$0^\circ$
<i>Critical angle</i> ( $\alpha_{cr}$ )	$8^\circ$	$6^\circ$	$4^\circ$
$f_{cr}$ (at $\alpha_{cr}$ )	1.28 Hz	3.56 Hz	9.34 Hz

Flow regions are compared with the regions defined by Huang and Lin (1995) for NACA 0012 airfoil at different Re numbers and angles of attack as shown

in Fig. 11. Region A represents *Attached Boundary Layer*, Region B represents *Separated Boundary Layer*



\*Region A: Attached Boundary Layer, Region B: Separated Boundary Layer, Region C: Boundary Layer Completely Separated defined by Huang and Lin (1995)

**Fig. 11. Reynolds number versus angle of attack map of NACA 0012 airfoil at low Reynolds numbers.**

Layer and Region C is denoted as the *Boundary Layer completely separated* region where the flow completely separates from the airfoil upper surface. From the numerical simulations given by Kunz and Kroo (2000), where they emphasized that they stopped the simulations when the steady convergence is not reached. From the simulations that they performed, it can be found that the critical angle is above  $7.5^\circ$  for  $Re=2000$  and above  $6^\circ$  for  $Re=6000$  for 8% thick NACA 0008 airfoil. They found critical angles almost same for NACA 0006 airfoil. The critical angle is above  $7^\circ$  for  $Re=2000$  and above  $5^\circ$  for  $Re=6000$  for NACA 0004. As they performed also simulations for 2% thick NACA 0002 airfoil, they stopped their analysis at  $5.5^\circ$ , which shows that the critical angle is above  $8^\circ$  for  $Re=1000$ , above  $5.5^\circ$  for  $Re=2000$  and above  $4^\circ$  for  $Re=6000$  for NACA 0002 (Table 3). A similar result is also found by Kurtulus (2016) for NACA 0002 airfoil at  $Re=1000$  where the critical angle is detected in the range of  $\alpha_{cr} \in [8^\circ \ 9^\circ]$ . It can be seen that the critical angle decreases as the Reynolds number increases. It is clear that the unsteadiness is delayed at higher angles of attack by the decrease of the Reynolds number which is also a result found in the current study (see Table 3). The transition angle from the continuous mode to alternating mode shedding has also been studied by Gopalakrishnan Meena *et al.* (2018) for symmetric NACA profiles for different thicknesses with and without Gurney flap at  $Re=1000$ . They compared their results with Kurtulus (2016) and found very similar results for NACA 0012 at  $Re=1000$ . Their findings about critical angle of attack is also tabulated in Table 3. Gopalakrishnan Meena *et al.* (2018) also performed 3D analysis and found that alternating shedding mode tend to remain two dimensional even with spanwise effects at these low angles of attack and Reynolds number.

Thickness decrease has an increasing tendency in critical angle for  $Re=1000$  ( $\alpha_{cr}=8^\circ$  for NACA 0012,  $8^\circ < \alpha_{cr} < 9^\circ$  for NACA 0002 and  $7^\circ < \alpha_{cr} < 8^\circ$  for NACA 0000). However, as the Reynolds number increases, the critical angle is found to have a decreasing trend for 12% thick NACA 0012 airfoil (Table 3). For  $Re=2000$ , the airfoil thickness is found to affect the critical angle with an increasing trend from 12% airfoil ( $5^\circ < \alpha_{cr} < 6^\circ$ ) to 6% airfoil thickness ( $\alpha_{cr} > 7.5^\circ$ ) then the critical angle has a decreasing trend towards the 4% ( $\alpha_{cr} > 7^\circ$ ) and 2% thick airfoils ( $\alpha_{cr} > 5.5^\circ$ ).

**Table 3 Critical angle at different Reynolds numbers and airfoil thicknesses in comparison with the literature data**

Re	t/c	Critical angle	Reference (E): Experimental (N): Numerical
1000	0.18	$\alpha_{cr} = 6^\circ$	Gopalakrishnan Meena <i>et al.</i> (2018) (N)
1000	0.12	$\alpha_{cr} = 8^\circ$	Kurtulus (2016) (N) Gopalakrishnan Meena <i>et al.</i> (2018) (N)
1200	0.12	$4 \leq \alpha_{cr} \leq 7^\circ$	Huang <i>et al.</i> (2001) (E)
2000	0.12	$5^\circ < \alpha_{cr} < 6^\circ$	Current study (N)
3195	0.12	$\alpha_{cr} = 4^\circ$	Huang and Lin (1995) (E)
4000	0.12	$3^\circ < \alpha_{cr} < 4^\circ$	Current study (N)
2000	0.08	$\alpha_{cr} > 7.5^\circ$	Kunz and Kroo (2000) (N)
6000	0.08	$\alpha_{cr} > 6^\circ$	Kunz and Kroo (2000) (N)
1000	0.06	$8^\circ < \alpha_{cr} < 9^\circ$	Gopalakrishnan Meena <i>et al.</i> (2018) (N)
2000	0.06	$\alpha_{cr} > 7.5^\circ$	Kunz and Kroo (2000) (N)
6000	0.06	$\alpha_{cr} > 6^\circ$	Kunz and Kroo (2000) (N)
2000	0.04	$\alpha_{cr} > 7^\circ$	Kunz and Kroo (2000) (N)
6000	0.04	$\alpha_{cr} > 5^\circ$	Kunz and Kroo (2000) (N)
1000	0.02	$8^\circ < \alpha_{cr} < 9^\circ$ $\alpha_{cr} > 8^\circ$	Kurtulus (2016) (N) Kunz and Kroo (2000) (N)
2000	0.02	$\alpha_{cr} > 5.5^\circ$	Kunz and Kroo (2000) (N)
6000	0.02	$\alpha_{cr} > 4^\circ$	Kunz and Kroo (2000) (N)
1000	0.00 (Flat plate)	$7^\circ < \alpha_{cr} < 8^\circ$	Gopalakrishnan Meena <i>et al.</i> (2018) (N)

### 3.2 Instantaneous Aerodynamic Force Coefficients and Flowfields

Instantaneous lift and drag coefficients for different Reynolds numbers investigated are presented in Fig. 12 for  $\alpha=0^\circ$  and  $\alpha=8^\circ$ . At  $\alpha=0^\circ$ , apart the impulsive

start interval, the unsteady lift and drag coefficients are found to be almost constant for  $Re=1000, 2000$  and  $4000$  (Fig. 12a). As the angle of attack increases to  $\alpha=8^\circ$ , the sinusoidal oscillations of the aerodynamic force coefficients are clearly visible for  $Re=2000$  and  $4000$  cases (Fig. 12b). The oscillatory behavior of the aerodynamic coefficients is mainly due to the both counterclockwise (CCW) trailing edge vortex and clockwise (CW) laminar separation bubble generated on the upper surface and their alternating shedding towards the downstream of the airfoil. The critical angle is denoted where the unsteady aerodynamic force coefficients exhibit an obvious unsteady oscillatory motion with an alternating vortex at the wake of the airfoil in addition to an amplitude spectrum of lift coefficient showing a distinguishable, a high amplitude peak value (see Fig. 15). It is found that for  $Re=1000$ , the critical angle of attack is  $8^\circ$ . The oscillation magnitude of the lift coefficient is  $-0.2\%$  smaller (minimum  $C_l$ ),  $+0.4\%$  bigger (maximum  $C_l$ ) than the mean value for  $Re=1000$ . These oscillations increase abruptly with Reynolds number to almost  $-10\%$  and  $+11\%$  of the mean value for  $Re=2000$  and  $-32\%$  and  $+39\%$  for  $Re=4000$ .

The attached laminar boundary layer, which is subject to an adverse pressure gradient, results a separation of the flow which creates a laminar

separation bubble on the airfoil surface at these low Reynolds numbers. For  $Re=2000$  and  $\alpha=8^\circ$  case, the instantaneous streamlines and pressure coefficient contours are shown close to the airfoil in Fig. 13 to reveal the alternating vortex behavior between the time interval [99.5s 100s]. The instantaneous force coefficients at this time interval are also presented with a close view in Fig. 14. At maximum lift, drag and lift to drag ratio (at  $t=99.5s$ ,  $C_{lmax}=0.3935$ ,  $C_{dmax}= 0.1211$ ), LSB (CW) is observed to start to detach from the upper surface of the airfoil (Fig. 13). The reattachment point at the trailing edge is pushed downstream of the airfoil and create a saddle point just downstream of the airfoil's trailing edge (Perry and Fairlie 1975). High suction pressure region is observed on the overall upper surface of the airfoil. At  $t=99.5s$ , a new trailing edge vortex is also observed to be formed due to the shear layer which curves from the lower surface towards the upper surface and it grows at the upper surface of the airfoil just at the trailing edge by pushing downstream the previously generated vortex (see  $t= [99.525s 99.60s]$  interval pressure contours in Fig. 13). The minimum lift coefficient is observed at  $t= 99.625s$  as shown in Fig. 14, where the trailing edge vortex grow and the LSB detaches from the airfoil surface (Fig. 13). This is also a time which is very close to the minimum drag coefficient point (Fig. 14).

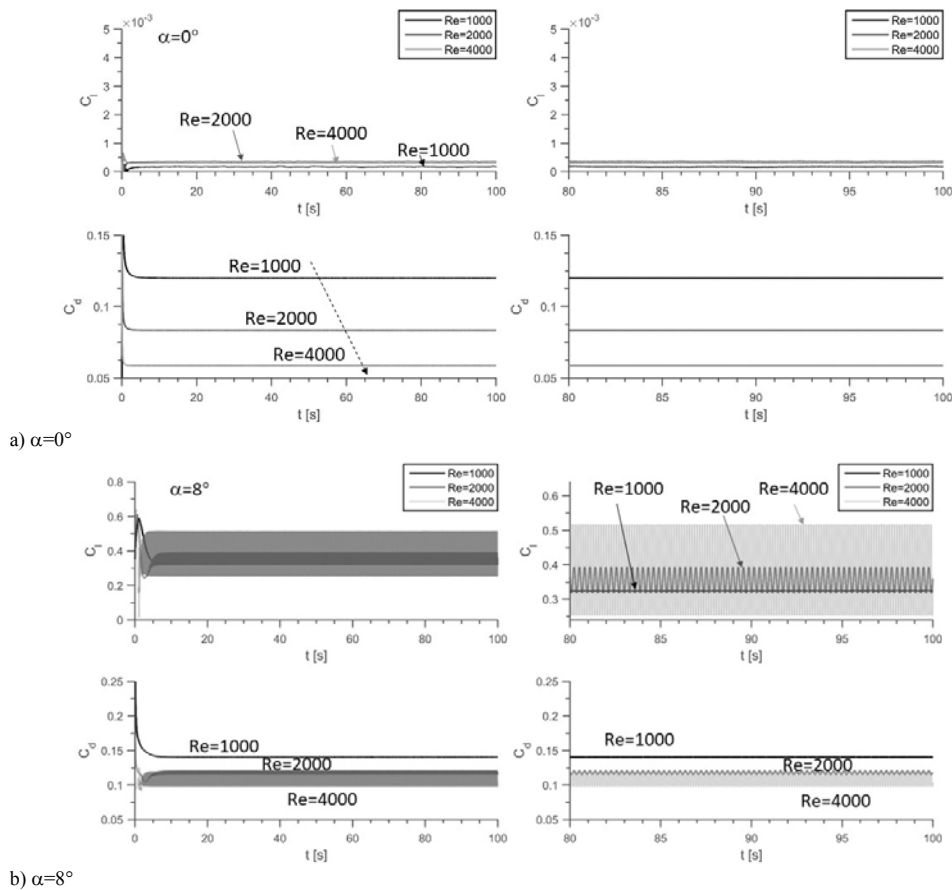


Fig. 12. Instantaneous lift and drag coefficients at different Reynolds numbers at a)  $\alpha=0^\circ$  and b)  $\alpha=8^\circ$ .

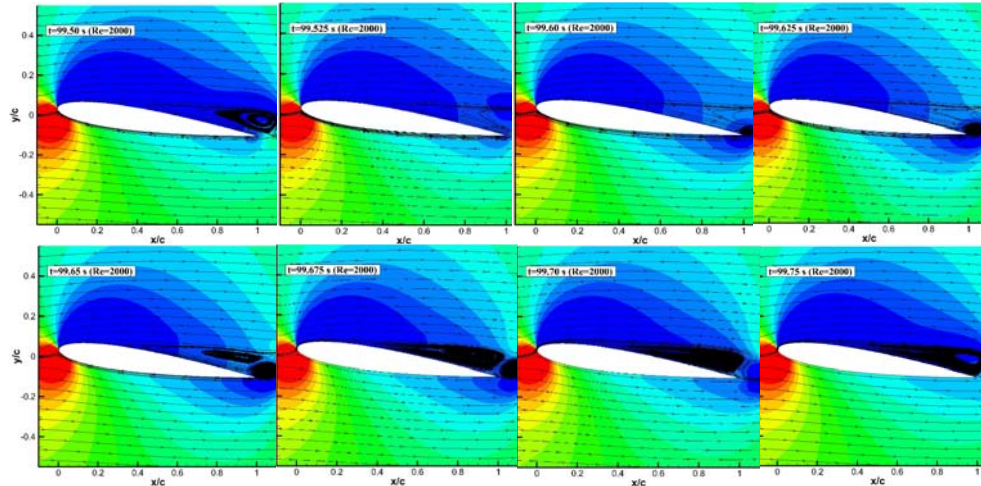


Fig. 13. Instantaneous streamlines and  $C_p$  contours at  $Re=2000$ ,  $\alpha=8^\circ$ .

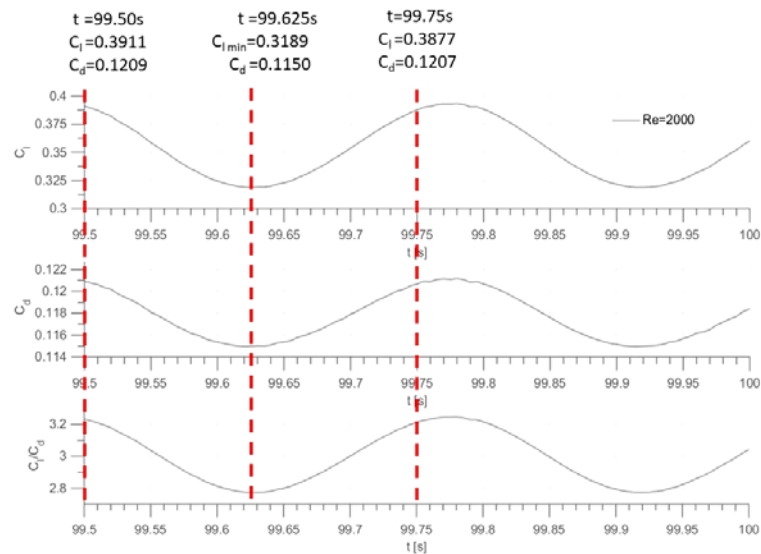


Fig. 14. Instantaneous  $C_l$ ,  $C_d$ ,  $C_l/C_d$  values at  $Re=2000$ ,  $\alpha=8^\circ$ .

At  $t=99.625s$ , as shown with the streamlines in Fig. 13, LSB is found to shed at the wake of the airfoil with a trace of LSB left behind it on the airfoil upper surface. At  $t=99.65s$ , LSB once more reattach to the upper surface of the airfoil and both trailing edge vortex and LSB is observable (Fig. 13). Both the lift and drag coefficients starts to increase from their minimum values until  $t=99.77s$  (Fig. 14). The reattachment point of the LSB shifts towards the trailing edge by resulting the trailing edge vortex (CCW) to be shed downstream as shown in Fig. 13 for  $t=99.75s$ . The LSB is now observed to settle on the upper surface of the airfoil with a clear reattachment at the trailing edge. With the periodic shedding of the LSB (CCW) and trailing edge vortices (CW) a sinusoidal pattern on the aerodynamic forces are observed and an alternating vortex pattern is seen behind the airfoil at the downstream. It should be noted that because

of the periodicity,  $C_p$  contours and streamlines at  $t=99.7s$  and  $t=100s$  are almost the same (Fig. 13-last column of 3<sup>rd</sup> and 4<sup>th</sup> rows).

### 3.3 Amplitude spectrum of the lift coefficient and fundamental frequency

The oscillations reveal a clear fundamental frequency in the amplitude spectra of the lift coefficients as can be seen from Fig. 15, specifically for angles greater than equal to critical angle of attack as was tabulated in Table 2. Above the critical angle, a clear fundamental frequency and its sub-harmonics are visible in the amplitude spectra of the lift coefficients (see Fig. 15 for  $\alpha=4^\circ$  at  $Re=4000$  with maximum fundamental frequency  $f_{cr}=9.34$  Hz, see Fig. 15 for  $\alpha=6^\circ$  at  $Re=2000$  with  $f_{cr}=3.56$  Hz and see Fig. 15 for  $\alpha=8^\circ$  at  $Re=1000$  with  $f_{cr}=1.28$  Hz).

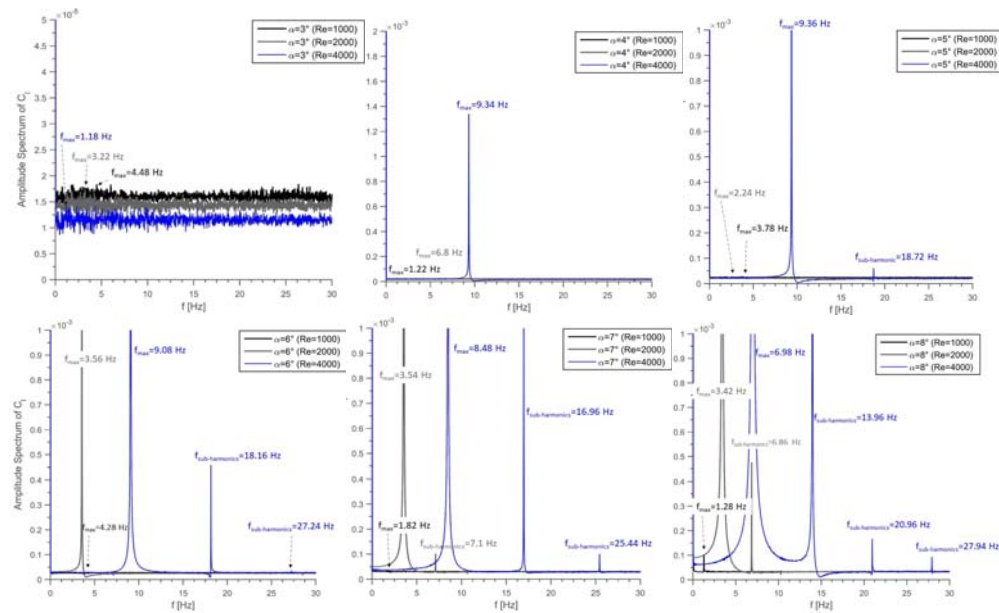


**Fig. 15.** Amplitude spectrum of  $C_l$  for NACA 0012 airfoil for  $3^\circ \leq \alpha \leq 8^\circ$  for different Reynolds numbers.

In the current study, more intension is also given to the frequency spectrum of the lift coefficient for the angles above *LSB formation angle* ( $\alpha_{LSB}$ ) which is  $4^\circ$  for  $Re=1000$ ,  $2^\circ$  for  $Re=2000$  and  $0^\circ$  for  $Re=4000$  (Table 2). The maximum amplitude frequency gives a very low amplitude frequency spectrum without a noticeable peak as shown in Fig. 15 (see for  $\alpha=3^\circ$ ).

#### 4. CONCLUSION

The flow behind NACA 0012 airfoil at low Reynolds numbers has been studied at low angles of attack for the  $Re=1000$ ,  $2000$  and  $4000$ . The transition from the steady condition to periodic force evolution has been revealed with a detailed flow field analysis. The *critical angle* from the steady convergence condition (Mode 1) to unsteady oscillatory behaviors (Mode 2) were previously obtained at  $\alpha=9^\circ$  for NACA 0002 and  $\alpha=8^\circ$  for NACA 0012 at  $Re=1000$ . The fundamental frequency of shedding for alternating vortices is evaluated for different Reynolds number at the critical angle of attack. Another solution obtained from the current study is that although the mean lift coefficient is not affected too much from the incremental change of the Reynolds number from  $1000$  to  $4000$  for NACA 0012 airfoil, the mean drag coefficient is found to decrease as the Reynolds number increases for the angles of attack less than equal to  $8^\circ$  even in the presence of a growing *LSB* at the trailing edge of the airfoil.

#### ACKNOWLEDGEMENTS

This work is supported by TUBITAK with project number 116M273.

#### REFERENCES

- Cleaver, D. J, Z. Wang and I. Gursul (2012). Bifurcating flows of plunging airfoils at high Strouhal numbers. *Journal of Fluid Mechanics* 708, 349-376.
- Council, J. N. N. and K. G. Boulama (2013). Low-Reynolds-number aerodynamic performances of the NACA 0012 and Selig-Donovan 7003 airfoils. *AIAA Journal* 50(1), 204–216.
- Durante, D., E. Rossi and A. Colagrossi (2020). Bifurcations and chaos transition of the flow over an airfoil at low Reynolds number varying the angle of attack. *Communications in Nonlinear Science and Numerical Simulation* 89, 2020.
- Eljack, E., J. Soria, Y. Elawad and T. Ohtake (2021). Simulation and characterization of the laminar separation bubble over a NACA-0012 airfoil as a function of angle of attack. *Physical Review Fluids* 6, 034701, 1-29.
- Eljack, M. E. and J. Soria (2020). Investigation of the low-frequency oscillations in the flowfield about an airfoil. *AIAA Journal* 58(10), 4271-4286.
- Gopalakrishnan Meena, M., K. Taira and K. Asai (2018). Airfoil-wake modification with Gurney flap at low Reynolds number. *AIAA Journal* 56(4), 1348-1359.
- Han, J. S, J. W. Chang and S. T. Kim (2014). Reynolds number dependency of an insect-based flapping wing. *Bioinspiration & Biomimetics* 9, 046012, 1-16.
- Hoarau, Y., M. Braza, Y. Ventikos, D. Faghani and G. Tzabiras (2003). Organized modes and the

- three dimensional transition to turbulence in the incompressible flow around a NACA0012 wing. *Journal of Fluid Mechanics*, 496, 63–72.
- Huang, R. F. and C. L. Lin (1995) Vortex Shedding and Shear-Layer Instability of Wing at Low-Reynolds Numbers. *AIAA Journal* 33, 1398-1403.
- Huang, R. F., J. Y. Wu, J. H. Jeng and R. C. Chen (2001). Surface flow and vortex shedding of an impulsively started wing. *Journal of Fluid Mechanics* 441, 265-292.
- Jones, B. M. (1933). An Experimental study of the stalling of wings. *Aeronautical Research Council TR 1588*.
- Khalid, M. S. U. and I. Akhtar (2012) Characteristics of flow past a symmetric airfoil at low Reynolds Number: A nonlinear perspective. *Proceedings of the ASME 2012 International Mechanical Engineering Congress & Exposition IMECE2012*, Houston, Texas, USA.
- Kunz, P. and I. Kroo (2000). Analysis and design of airfoils for usqe at ultra-low Reynolds numbers. In T.J. Mueller (Ed.) *Proceedings of AIAA fixed, flapping and rotary wing vehicles at very low Reynolds numbers conference*. AIAA, Notre Dame, 349–372.
- Kurtulus, D. F. (2015). On the unsteady behavior of the flow around NACA 0012 airfoil with steady external conditions at  $Re=1000$ . *International Journal of Micro Air Vehicles* 7(3), 301-326.
- Kurtulus, D. F. (2016). On the wake pattern of symmetric airfoils for different incidence angles at  $Re=1000$ . *International Journal of Micro Air Vehicles* 8 (2), 109-139.
- Kurtulus, D. F. (2018). Aerodynamic loads of small amplitude pitching NACA 0012 airfoil at Reynolds Number of 1000. *AIAA Journal* 56(8), 3328-3331.
- Kurtulus, D. F. (2019). Unsteady aerodynamics of a pitching NACA 0012 airfoil at low Reynolds number. *International Journal of Micro Air Vehicles* 11, 1-21.
- Lee, H. W. and R. F. Huang (1998). Frequency selection of wake flow behind a NACA 0012 wing. *Journal of Marine Science and Technology* 6(1), 29-37.
- Liu, Y., K. Li, J. Zhang, H. Wang and L. Liu (2012). Numerical bifurcation analysis of static stall of airfoil and dynamic stall under unsteady perturbation. *Commun Nonlinear Sci Numer Simulat* 17, 3427–3434.
- Mittal, S. and T. E. Tezduyar (1994). Massively parallel finite element computation of incompressible flows involving fluid-body interactions. *Computer Methods in Applied Mechanics and Engineering* 112, 253-282.
- Nakhchi, M. E., S. Win Naung and M. Rahmati (2021) High-resolution direct numerical simulations of flow structure and aerodynamic performance of wind turbine airfoil at wide range of Reynolds numbers, *Energy* 225, 120261.
- Ohtake, T., Y. Nakae and T. Motohashi (2007). Nonlinearity of the aerodynamic characteristics of NACA0012 aerofoil at low Reynolds numbers. *Journal of the Japan Society for Aeronautical and Space Sciences* 55(644), 439–445.
- Perry, A. E. and B. D. Fairlie (1975) Critical points in flow patterns, In F.N. Frenkiel, R.E. Munn (Ed.). *Advances in Geophysics*, Elsevier 18, Part B, 299-315.
- Rossi, E., A. Colagrossi, G. Oger and D. Le Touzé (2018) Multiple bifurcations of the flow over stalled airfoils when changing the Reynolds number. *Journal of Fluid Mechanics* 846, 356-391.
- Schmitz, F. W. (1967). Aerodynamics of the model airplane. Part 1. Airfoil measurements. NACA-TM-X-60976.
- Sunada, S., A. Sakaguchi and K. Kawaguchi (1997). Airfoil section characteristics at low Reynolds number. *Journal of Fluids Engineering* 119, 129-135.
- Suzuki, T., H. Ji and F. Yamamoto (2009) Unsteady PTV velocity field past an airfoil solved with DNS: Part 1. Algorithm of hybrid simulation and hybrid velocity field at  $Re=10^3$ . *Experiments in Fluids* 47, 957–976.
- Tani, I. (1964). Low-speed flows involving bubble separations. *Progress in Aerospace Sciences*, 5, 70-103.
- Traub, L. W. and E. Cooper (2008) Experimental Investigation of Pressure Measurement and Airfoil Characteristics at Low Reynolds Numbers. *Journal of Aircraft* 45(4), 1322–1333.
- Traub, L. W. and C. Coffman (2019). Efficient low-Reynolds-number airfoils. *Journal of Aircraft* 56 (5), 1987-2003.
- Watmuff, J. H. (1999) Evolution of a wave packet into vortex loops in a laminar separation bubble. *Journal of Fluid Mechanics* 397, 119–169.